Multidecadal ENSO Amplitude Variability in a 1000-yr Simulation of a Coupled Global Climate Model: Implications for Observed ENSO Variability

SIMON BORLACE AND WENJU CAI

CSIRO Marine and Atmospheric Research, Aspendale, Victoria, Australia

AGUS SANTOSO

Climate Change Research Centre, and ARC Centre of Excellence for Climate System Science, University of New South Wales, New South Wales, Australia

(Manuscript received 20 May 2013, in final form 13 September 2013)

ABSTRACT

The amplitude of the El Niño–Southern Oscillation (ENSO) can vary naturally over multidecadal time scales and can be influenced by climate change. However, determining the mechanism for this variation is difficult because of the paucity of observations over such long time scales. Using a 1000-yr integration of a coupled global climate model and a linear stability analysis, it is demonstrated that multidecadal modulation of ENSO amplitude can be driven by variations in the governing dynamics. In this model, the modulation is controlled by the underlying thermocline feedback mechanism, which in turn is governed by the response of the oceanic thermocline slope across the equatorial Pacific to changes in the overlying basinwide zonal winds. Furthermore, the episodic strengthening and weakening of this coupled interaction is shown to be linked to the slowly varying background climate. In comparison with the model statistics, the recent change of ENSO amplitude in observations appears to be still within the range of natural variability. This is despite the apparent warming trend in the mean climate. Hence, this study suggests that it may be difficult to infer a climate change signal from changes in ENSO amplitude alone, particularly given the presently limited observational data.

1. Introduction

El Niño–Southern Oscillation (ENSO) is one of the most important sources of natural climatic variability. On a time scale of 2–7 yr, the eastern equatorial Pacific varies between anomalously cold (La Niña) and warm (El Niño) conditions (McPhaden et al. 2011). The associated sea surface temperature (SST) anomalies strongly influence climate extremes around the globe (e.g., Vos et al. 1999; Changnon 1999; Li et al. 2011; Vincent et al. 2011; Cai et al. 2012). Since the late twentieth century there has been an increase in the observed ENSO amplitude (see Fig. 2a). There is an ongoing debate as to whether the increased amplitude since the late twentieth century is a response to greenhouse warming (Guilyardi et al. 2009; Collins et al. 2010). Over the last decade the trade winds have strengthened, and the thermocline is more steeply tilted down to the west in the tropical Pacific (McPhaden et al. 2011). Such changes in the background mean state are not consistent with those expected as a result of greenhouse warming (Yeh et al. 2009) and hence suggest that natural variability modulates ENSO amplitude over multidecadal time scales.

An 1100-yr paleo-proxy time series from tree rings shows that ENSO amplitude varies over a quasi-regular cycle of 50–90 yr (Li et al. 2011). It is accepted that study of variability of ENSO amplitude requires a time series longer than 500 yr (Wittenberg 2009). Furthermore, understanding the underlying processes demands an analysis of the full dynamics. Coupled global climate models (CGCMs) are thus an invaluable tool. Modeling studies have shown that even in the absence of greenhouse warming, ENSO amplitude varies over multidecadal time scales because of natural modulations (Rodgers et al. 2004; Wittenberg 2009; Deser et al. 2012). While various studies have offered possible factors that can influence multidecadal variability in ENSO amplitude [see, e.g., Lopez et al. (2013), and references therein], none has attempted to investigate this by considering the

Corresponding author address: Simon Borlace, CSIRO Marine and Atmospheric Research, PMB 1, Aspendale VIC 3195, Australia.
E-mail: simon.borlace@csiro.au

DOI: 10.1175/JCLI-D-13-00281.1

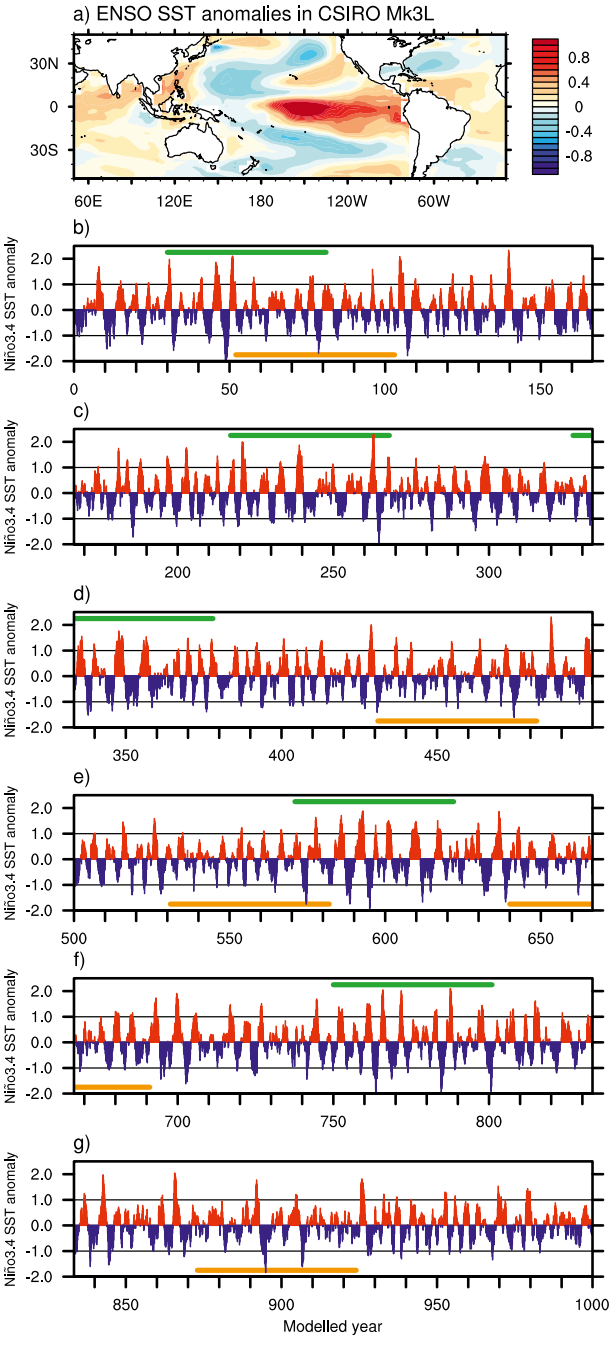

FIG. 1. (a) Spatial map of the regression between sea surface temperature and the Niño-3.4 region (5°N–5°S, 170°–120°W) SST anomaly for the CSIRO Mk3L CGCM. (b)–(g) Time series of Niño-3.4 region sea surface temperature (SST) anomaly for the 1000-yr integration (corresponding to model years 3000–4000) of the CSIRO Mk3L CGCM. The 51-yr epochs of high ENSO variability are highlighted by the green lines and epochs of low ENSO variability are highlighted by the orange lines.

relative importance of all of the underlying feedback processes, each of which is a function of background state and air–sea interactions.

Despite the continuing debate on whether irregularity in ENSO evolution arises resulting from stochastic forcing or intrinsic chaotic dynamics of the coupled system (see, e.g., Neelin et al. 1998), it is clear that ENSO variability arises from competition between positive and negative feedback processes, involving coupled interactions among the wind, SST, and thermocline depth in the tropical Pacific Ocean (termed Bjerknes feedback; Bjerknes 1969), and damping because of air–sea heat fluxes and ocean currents. Jin et al. (2006) formulated a Bjerknes (BJ) coupled stability index in the context of the recharge/discharge oscillator (Jin 1997) to express ENSO linear growth rate in terms of these feedback processes and the mean climate. Another version of the formula can be found in Kim and Jin (2011a). Although the recharge–discharge paradigm does not capture every element of ENSO behavior (e.g., McGregor et al. 2013), it does represent the overall ENSO physics, which are grossly linear. As such, the formulation has been found useful to study the impact of a mean state change on ENSO behavior (e.g., Santoso et al. 2011) and the balance of feedback processes across CGCMs (Kim and Jin 2011b; Santoso et al. 2012; Kim et al. 2013) and reanalysis products (Lübbecke and McPhaden 2013).

Here we utilize a long integration of a coupled climate model and the BJ index formula to illustrate that multidecadal vacillation in ENSO amplitude, which is of comparable size to the observed, can be traced to a dynamical process involving thermocline depth and winds that varies naturally in strength over these long time scales.

2. Models and data

The Commonwealth Scientific and Industrial Research Organisation Mark 3L (CSIRO Mk3L) is a fully coupled model designed for millennial-scale climate simulation (Phipps 2010). The atmospheric model resolution is 5.6° (zonal) × 3.2° (meridional), with 18 vertical levels. The ocean model resolution is 2.8° × 1.6° with 21 vertical levels of increasing thickness with depth. The model version used here is that of Santoso et al. (2012) with an improved representation of the Indonesian Throughflow gateway. The model is forced with atmospheric CO_2 concentrations fixed at preindustrial levels (280 ppm) and integrated over 4000 yr. To maintain a realistic background mean state, a flux adjustment is applied to heat, freshwater, and momentum that is seasonally varying but annually fixed. It is therefore constant over multidecadal periods and does not influence

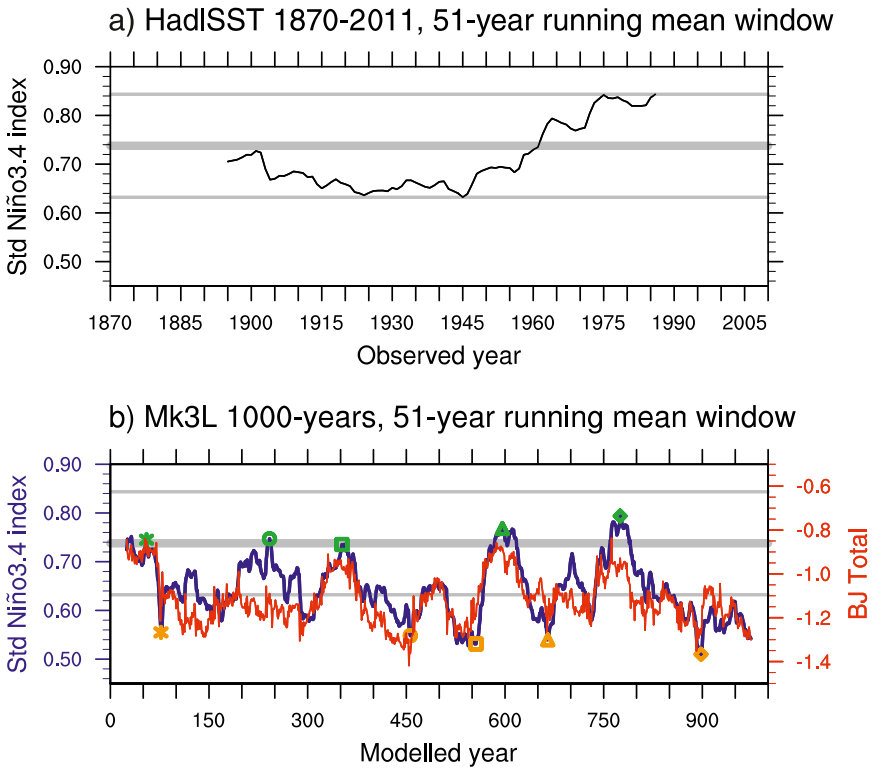

FIG. 2. (a) Observed ENSO magnitude (°C), which is defined as the standard deviation of the Niño-3.4 region (5°N–5°S, 170°–120°W) calculated over a 51-yr sliding window that is shifted forward every year. The 51-yr window is centered at the year labeled. (b) ENSO variability over a 51-yr window as simulated by the CSIRO Mk3L CGCM (blue line), and the corresponding BJ stability index (red line, yr^{-1}) calculated over the same 51-yr window. Epochs of high ENSO variability (green markers) and low ENSO variability (orange markers) are highlighted. The thin horizontal lines in both panels correspond to the minimum and maximum observed value, while the thick horizontal lines correspond to the mean.

the modulation of ENSO amplitude. The last 1000 yr of integration, by which the model climate has reached a stable state, are analyzed. Variables have been linearly detrended prior to analysis to ensure that model drift, which is in any case minor, is excluded.

As already discussed by Santoso et al. (2012), the model simulates ENSO with reasonable degree of realism, despite the biases that are also prevalent in many other climate models (Guilyardi et al. 2009). The simulated ENSO SST anomalies (Fig. 1a) extend farther west than observed, associated with the cold tongue bias linked to overly strong trade winds. In addition, the simulated ENSO is of weaker magnitude and slightly longer period than observed, given the coarse model resolution, but are still within the observed range [see Santoso et al. (2012), their Fig. 3]. As shown in Figs. 1b–g, the modeled ENSO does exhibit apparent irregularity in amplitude, making it suitable for studying its multidecadal variability.

To diagnose multidecadal variation in ENSO amplitude we calculate the standard deviation of SST anomaly over the Niño-3.4 region (5°S–5°N, 170°–120°W) over a 51-yr sliding window. The size of the sliding window is chosen to sufficiently sample the simulated ENSO variability (Santoso et al. 2012) while allowing a direct comparison with the relatively short observational data [1870–2011 Hadley Centre Sea Ice and Sea Surface Temperature dataset (HadISST); Rayner et al. 2003]. Note that our model results do not deviate much when we use a window size of 101 yr (not shown). It should be stressed that while our model and the stability analysis are similar to those adopted by Santoso et al. (2011, 2012), the sliding-window approach used here is specifically designed for unraveling the mechanisms for the multidecadal variability in ENSO magnitude, which was not the focus of those earlier studies.

3. Observed and simulated ENSO magnitude

The observed ENSO amplitude increases from a standard deviation (std) value of 0.63°C early of the twentieth

TABLE 1. Overview of the Bjerknes stability index formulated by Kim and Jin (2011a). The first term on the right-hand side represents the total Bjerknes (BJ) stability index, and the second term (ε) corresponds to the rate that the ocean adjusts to damping processes. Volume averaged quantities over the eastern region or western region of the equatorial Pacific basin are denoted using $\langle A \rangle$, and are distinguished in the table by the subscripts E and W, respectively. Volume and area-averaged background mean state variables and anomalies are calculated over 5°N–5°S, 120°E–170°W for a western region and 5°N–5°S, 170°–90°W for an eastern region across the equatorial Pacific, and the upper 50 m is considered for the calculation of volume-averaged ocean variables. Area-averaged background mean state variables are expressed with an overbar, and T represents anomalous temperature.

$$2\mathrm{BJ} + \varepsilon = -\left(a_1 \frac{\langle \Delta \overline{u} \rangle_E}{L_x} + a_2 \frac{\langle \Delta \overline{v} \rangle_E}{L_y}\right) - \alpha_s + \mu_a \beta_u \left\langle -\frac{\partial \overline{T}}{\partial x} \right\rangle_E + \mu_a \beta_w \left\langle -\frac{\partial \overline{T}}{\partial z} \right\rangle_E + \mu_a \beta_h \left\langle \frac{\overline{w}}{H_1} \right\rangle_E a_h$$

Parameter	Description
$\overline{u}, \overline{v}, \overline{w}$	Mean zonal, meridional, and vertical velocity
L_x, L_y	Longitudinal and latitudinal length of the eastern box
a_1, a_2	Anomalous SSTs averaged at the boundaries and over the area of a region
H_1	Ocean mixed layer depth
$\partial \overline{T}/\partial x$	Mean zonal ocean temperature gradient
$\partial \overline{T}/\partial z$	Mean vertical ocean temperature gradient
α_s	Thermodynamic damping
μ_a	A wind response to a SST forcing
β_u	A response of an ocean surface zonal current to a wind forcing
β_w	A response of an ocean upwelling to a wind forcing
β_h	A response of the zonal slope of the equatorial thermocline to a wind forcing
a_h	An effect of the thermocline depth changes on ocean subsurface temperatures

century to 0.84°C toward the end of the century (Fig. 2a), corresponding to a difference of 0.21°C. The increase is consistent with Deser et al. (2012) but differs slightly because of the different sliding window. The simulated ENSO amplitude (Fig. 2b) is overall weaker than the observed, varying between 0.54° and 0.78°C. This largely stems from mean state biases, particularly the tendency for the thermocline to be too deep (not shown), which would weaken air–sea coupling (Santoso et al. 2011). Nonetheless, the interepoch difference (~0.24°C) is comparable with observations (~0.21°C), suggesting that the recent observed increase in ENSO amplitude may be still within the range of multidecadal variability. What processes govern these multidecadal fluctuations in ENSO amplitude?

4. Underlying processes behind ENSO amplitude modulation

The Kim and Jin (2011a) BJ stability index is used to measure the contributions of the various feedback processes during epochs of enhanced or reduced ENSO variability. A positive (negative) BJ stability index indicates a growth (decay) of ENSO variability. Positive contributions come from feedbacks associated with variations in zonal advection, Ekman pumping, and thermocline depth across the equatorial Pacific Ocean, while negative contributions come from damping by mean advection and net air–sea heat fluxes.

The formula elegantly expresses the feedbacks in terms of background mean states and a series of coupling coefficients as a measure of the strength of air–sea interactions (Table 1). The coupling coefficients are estimated using least squares regression using monthly time series (Santoso et al. 2011, 2012). The climatological seasonal cycle and variance longer than 7 yr are removed to focus on interannual anomalies.

Since the time series of the BJ stability index (Fig. 2b) and ENSO amplitude (Fig. 3a) are highly correlated (r = 0.73), the index and the contributing components are useful for diagnosing feedbacks associated with the multidecadal modulation of ENSO amplitude. The total index is overall negative (Fig. 3a) as it is dominated by the large damping by the mean advection (Fig. 3b) and air–sea heat fluxes (Fig. 3c), causing the simulated ENSO to be strongly damped. However, there are no significant relationships between these damping terms and ENSO amplitude, suggesting that neither of these damping processes controls the multidecadal variation in ENSO amplitude. On the other hand, each of the positive feedback terms and the ENSO amplitude variability are significantly correlated (Figs. 3d–f), the strongest correlation being with the thermocline feedback (r = 0.82). Thus the thermocline feedback is the dominant factor for the modeled multidecadal variability of ENSO amplitude.

a. Factors underpinning the dominance of the thermocline feedback

The thermocline feedback describes mean vertical advection of anomalous subsurface temperature, which is linked to thermocline depth variability, and is expressed

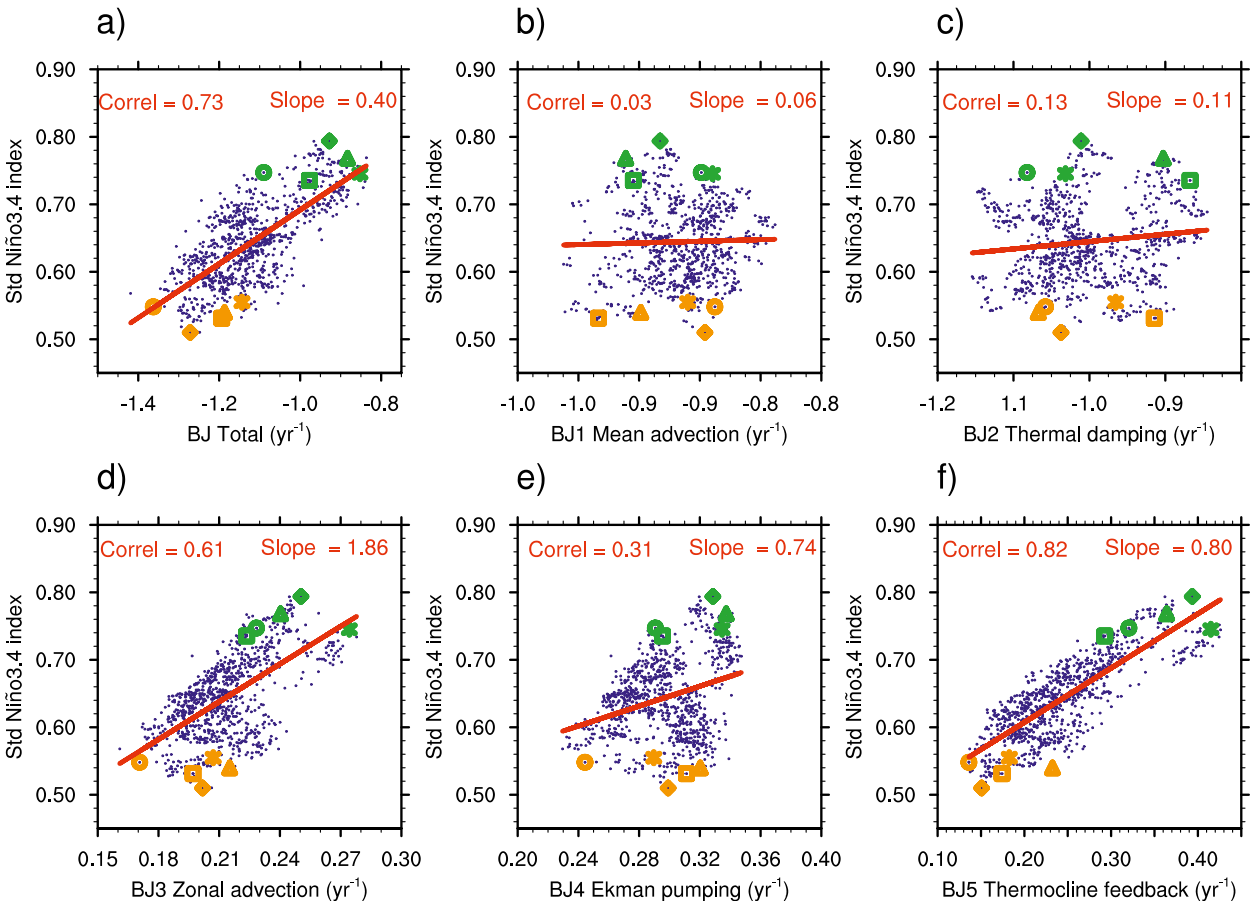

FIG. 3. Amplitude of the simulated ENSO, which is defined as the standard deviation of the Niño-3.4 index over a 51-yr sliding window vs (a) total BJ stability index, (b) damping by mean advection, (c) damping by air–sea heat fluxes, (d) zonal advective feedback, (e) Ekman pumping feedback, and (f) thermocline feedback. Epochs of high ENSO variability (green markers) and low ENSO variability (orange markers) are highlighted.

in terms of several ocean–atmosphere coupling coefficients (Jin et al. 2006). These coupling coefficients include the response of basinwide zonal winds to SST change in the east μ_a, the response of the equatorial thermocline slope to basinwide zonal wind stress change β_h, and the effect of thermocline depth changes on ocean subsurface temperatures in the east a_h (Table 1). The relationships between each of these parameters and the thermocline feedback term are shown in Figs. 4a–d, showing weak correlations for the background mean upwelling (Fig. 4c), μ_a (Fig. 4a), and a_h (Fig. 4d). The variations in the thermocline feedback term are essentially dominated by the β_h coefficient with a correlation of near unity (0.96; Fig. 4b). Therefore, it is the coupling between the equatorial thermocline slope and the basinwide zonal wind that drives the multidecadal modulation of ENSO amplitude in the model via the thermocline feedback.

The sensitivity of β_h is a product of their correlation and the ratio of their standard deviations. An increase in their coherence (i.e., stronger easterly wind anomalies correspond with stronger east–west thermocline slope) and/or stronger increase in the variability of the thermocline slope relative to that of the wind stress contributes to a stronger sensitivity. The correlation (0.98) between the thermocline feedback and the coherence (Fig. 4e) is remarkable, suggesting that during multidecadal periods when the equatorial thermocline slope and basinwide zonal wind stress display a strong coherence, there is a greater thermocline feedback and hence greater ENSO amplitude. There is also a significant correlation (0.68) between the standard deviation ratio and the thermocline feedback (Fig. 4f); however, it is the coherence between the two variables that contributes most to variability of the thermocline feedback on multidecadal time scales.

b. *Link to mean climate*

The above analysis demonstrates that the coherence between basinwide zonal wind stress and the thermocline slope controls the thermocline feedback in the

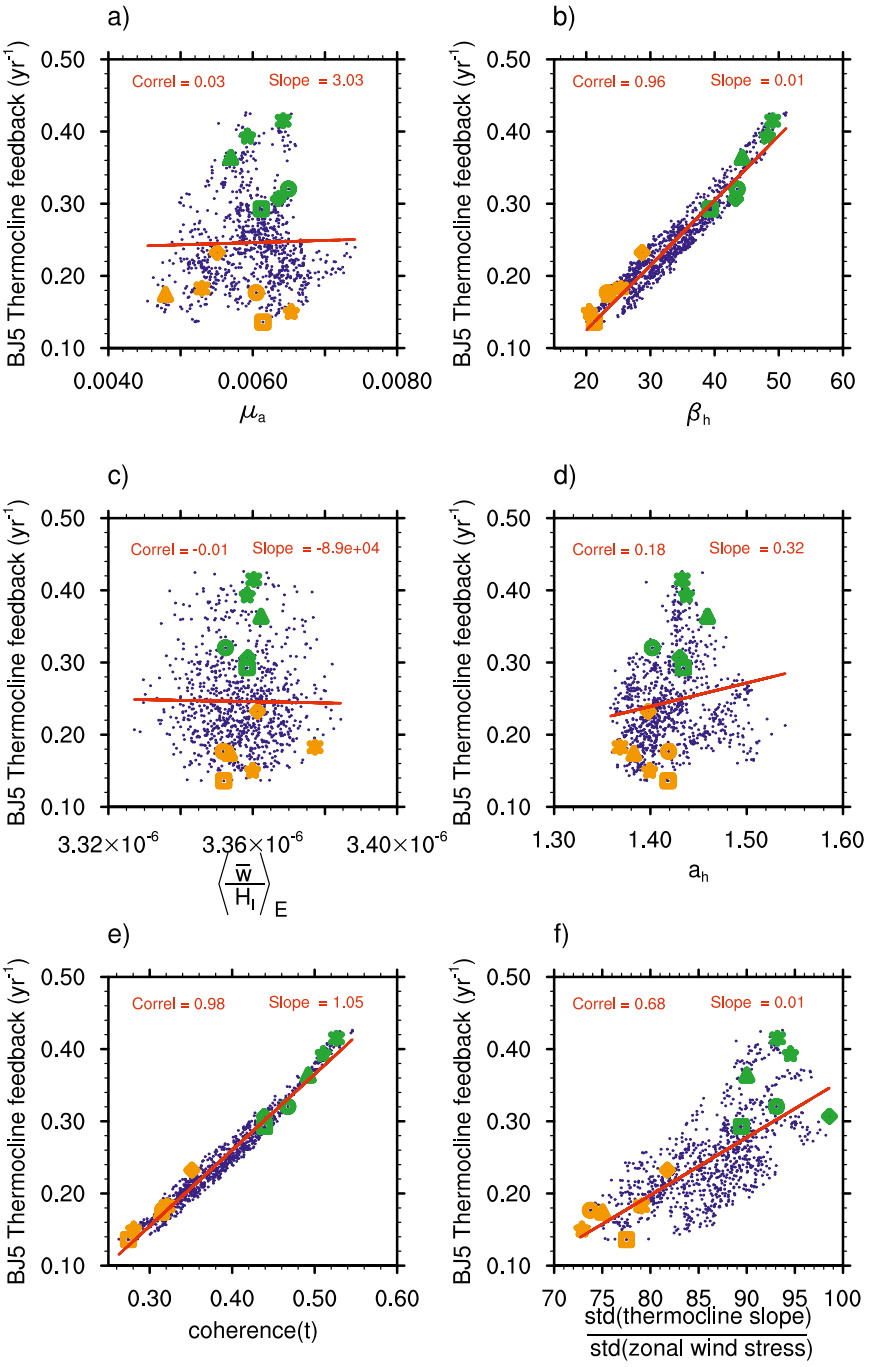

FIG. 4. The simulated thermocline feedback over a 51-yr sliding window vs (a) sensitivity of μ_a, (b) sensitivity of β_h, (c) mean upwelling, (d) sensitivity of a_h, (e) the coherence between the equatorial thermocline slope and basinwide zonal wind stress, and (f) the ratio of the standard deviations of the equatorial thermocline slope and the basinwide zonal wind stress. Epochs of high ENSO variability (green markers) and low ENSO variability (orange markers) are highlighted.

model. Here we reveal that this is associated with an evolving mean state. Correlation between the coherence time series and evolution of the mean state at each grid point, obtained by averaging over the same 51-yr sliding window, shows that during epochs of an enhanced coherence (and hence a stronger thermocline feedback and larger ENSO amplitude), climatological easterlies over the western equatorial Pacific are stronger (Fig. 5a),

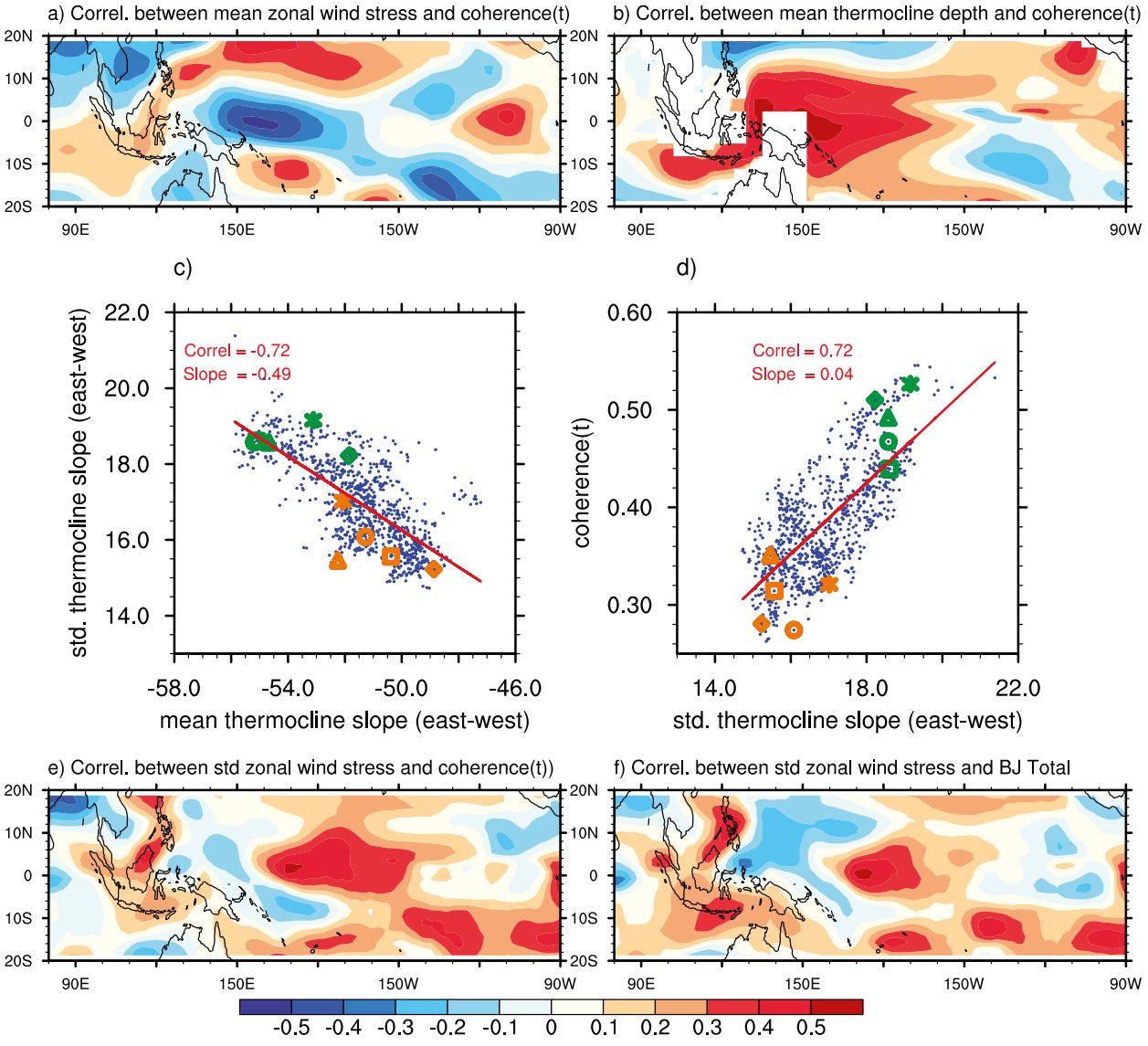

FIG. 5. Spatial map of the correlation between evolutions of the coherence (correlation) between the equatorial thermocline slope to basinwide zonal wind stress and (a) evolution of gridpoint mean zonal winds, and (b) gridpoint mean thermocline depth, all calculated using a 51-yr sliding window. (c) Time series of mean slope of the equatorial thermocline against time series of the variance of the thermocline slope, similarly calculated using a 51-yr sliding window, and (d) time series of the coherence against time series of the variance of the thermocline slope. Spatial map of the correlation of the evolution of variance of the gridpoint zonal wind stress with (e) the evolution of the coherence and (f) and the evolution of the total BJ stability index, again calculated using a 51-yr sliding window.

deepening the thermocline in the western equatorial Pacific (Fig. 5b) and creating a steeper thermocline slope across the basin. Thus, the steeper the mean thermocline slope the greater the variability of the thermocline slope (Fig. 5c), and in turn the more enhanced coherence between the basinwide zonal wind stress and the thermocline slope (Fig. 5d).

Correlations between the evolution of the coherence and the evolution of the gridpoint zonal wind stress variance reveal an enhanced variance of zonal wind stress anomalies in the central Pacific (Fig. 5e). This is expected because with stronger ENSO amplitude, the wind anomalies over this region, which are westerly during El Niño and easterly during La Niña, are also stronger. Interestingly, there is a tendency for decreased zonal wind variability in the western Pacific, as indicated by a negative (albeit weak) correlation. This negative correlation strengthens when the BJ total time series (red curve in Fig. 2b) is used instead (Fig. 5f). Easterly wind anomalies during an El Niño phase tend to damp warm SST

anomalies by forcing eastward propagating upwelling Kelvin waves that cool the surface and promote a transition toward La Niña (Weisberg and Wang 1997; Wang et al. 1999; Rodgers et al. 2004, Santoso et al. 2012). The decreased zonal wind variance over the western Pacific signifies a reduction in ENSO damping, and is therefore consistent with enhanced ENSO amplitude. Thus, the multidecadal ENSO amplitude modulation could occur with variations in the mean climate according to the extent of the wind–thermocline coupling.

5. Conclusions

The present study investigates the relative contribution of various ENSO feedback processes to the modulation of ENSO variability in a 1000-yr simulation of a coupled model. This modulation is governed by variations in the strength of the thermocline feedback, which is in turn controlled by the coherence between the basinwide zonal wind stress and the equatorial thermocline slope. During periods of enhanced coherence, a stronger mean easterly zonal wind stress in the western equatorial Pacific drives a steeper west–east slope of the thermocline across the basin. A tendency toward this mean state is associated with stronger variability in the east–west thermocline slope and zonal wind over the central Pacific, stronger thermocline feedback, and thus stronger ENSO amplitude in the model. In addition, there is a tendency for weaker zonal wind variability in the western Pacific, which leads to a weaker damping during ENSO. Our results demonstrate that multidecadal variation in ENSO amplitude can arise from episodic strengthening and weakening of a certain dynamic, such as the thermocline feedback in the model, linked to the slowly varying background climate.

While the debate continues as to how ENSO may change in a warming climate (Collins et al. 2010), climate models that are able to simulate realistic ENSO have shown that ENSO amplitude fluctuates over decadal and centennial time scales even in the absence of greenhouse warming (Rodgers et al. 2004; Wittenberg 2009; Deser et al. 2012), pointing to a role of natural variability. This makes detection of climate change influence on ENSO difficult.

The amplitude of ENSO events has clearly increased during the late twentieth century, along with an accelerating warming trend in the mean climate (Deser et al. 2012). However, we found that the observed modulation of ENSO amplitude is comparable in magnitude to that of the model, suggesting that the recent increase in observed ENSO strength may still be within the range of natural variability. Given the clearly warming climate, this implies that diagnostics other than ENSO amplitude need to be used to infer climate change signal, particularly given the limited observations and the sensitivity of ENSO amplitude to stochastic forcing (e.g., Aiken et al. 2013). In addition, since there is a significant direct relationship between ENSO amplitude and the linear dynamical feedbacks, as demonstrated here, it appears necessary to expand ENSO theory to account for the full behavior of ENSO beyond a linear paradigm.

Acknowledgments. This work is supported by the Australian Climate Change Science Program. We thank Seon Tae Kim and Won Moo Kim for reviewing the manuscript before submission. Agus Santoso is supported by the Australian Research Council.

REFERENCES

Aiken, C. M., A. Santoso, S. McGregor, and M. H. England, 2013: The 1970's shift in ENSO dynamics: A linear inverse model perspective. *Geophys. Res. Lett.,* **40,** 1612–1617, doi:10.1002/grl.50264.

Bjerknes, J., 1969: Atmospheric teleconnections from the equatorial Pacific. *Mon. Wea. Rev.,* **97,** 163–172.

Cai, W., and Coauthors, 2012: More extreme swings of the South Pacific convergence zone due to greenhouse warming. *Nature,* **488,** 365–369.

Changnon, S. A., 1999: Impacts of 1997–98 El Niño generated weather in the United States. *Bull. Amer. Meteor. Soc.,* **80,** 1819–1827.

Collins, M., and Coauthors, 2010: The impact of global warming on the tropical Pacific Ocean and El Niño. *Nat. Geosci.,* **3,** 391–397.

Deser, C., and Coauthors, 2012: ENSO and Pacific decadal variability in the Community Climate System Model version 4. *J. Climate,* **25,** 2622–2651.

Guilyardi, E., A. Wittenberg, A. Fedorov, M. Collins, C. Wang, A. Capotondi, G. J. van Oldenborgh, and T. Stockdale, 2009: Understanding El Niño in ocean–atmosphere general circulation models: Progress and challenges. *Bull. Amer. Meteor. Soc.,* **90,** 325–340.

Jin, F.-F., 1997: An equatorial ocean recharge paradigm for ENSO. Part I: Conceptual model. *J. Atmos. Sci.,* **54,** 811–829.

——, S. T. Kim, and L. Bejarano, 2006: A coupled-stability index for ENSO. *Geophys. Res. Lett.,* **33,** L23708, doi:10.1029/2006GL027221.

Kim, S. T., and F.-F. Jin, 2011a: An ENSO stability analysis. Part I: Results from a hybrid coupled model. *Climate Dyn.,* **36,** 1593–1607, doi:10.1007/s00382-010-0796-0.

——, and ——, 2011b: An ENSO stability analysis. Part II: Results from the twentieth and twenty-first century simulations of the CMIP3 models. *Climate Dyn.,* **36,** 1609–1627, doi:10.1007/s00382-010-0872-5.

——, W. Cai, F.-F. Jin, and J.-Y. Yu, 2013: ENSO stability in coupled climate models and its association with mean state. *Climate Dyn.,* doi:10.1007/s00382-013-1833-6.

Li, J., S.-P. Xie, E. R. Cook, G. Huang, R. D'Arrigo, F. Liu, J. Ma, and X.-T. Zheng, 2011: Interdecadal modulation of El Niño amplitude during the past millennium. *Nat. Climate Change,* **1,** 114–118.

Lopez, H., B. P. Kirtman, E. Tziperman, and G. Gebbie, 2013: Impact of interactive westerly wind bursts on CCSM3. *Dyn. Atmos. Oceans,* **59,** 24–51.

Lübbecke, J. F., and M. J. McPhaden, 2013: A comparative stability analysis of Atlantic and Pacific Niño modes. *J. Climate,* **26,** 5965–5980.

McGregor, S., N. Ramesh, P. Spence, M. H. England, M. J. McPhaden, and A. Santoso, 2013: Meridional movement of wind anomalies during ENSO events and their role in event termination. *Geophys. Res. Lett.,* **40,** 749–754, doi:10.1002/grl.50136.

McPhaden, M. J., T. Lee, and D. McClurg, 2011: El Niño and it relationship to changing background conditions in the tropical Pacific Ocean. *Geophys. Res. Lett.,* **38,** L15709, doi:10.1029/2011GL048275.

Neelin, J. D., D. S. Battisti, A. C. Hirst, F.-F. Jin, Y. Wakata, T. Yamagata, and S. E. Zebiak, 1998: ENSO theory. *J. Geophys. Res.,* **103** (C7), 14 261–14 290.

Phipps, S. J., 2010: The CSIRO Mk3L climate system model v1.2. Antarctic Climate and Ecosystems Cooperative Research Centre Tech. Rep. 4, 121 pp.

Rayner, N. A., D. E. Parker, E. B. Horton, C. K. Folland, L. V. Alexander, D. P. Rowell, E. C. Kent, and A. Kaplan, 2003: Global analyses of sea surface temperature, sea ice, and night marine air temperature since the late nineteenth century. *J. Geophys. Res.,* **108** (D14), 4407, doi:10.1029/2002JD002670.

Rodgers, K. B., P. Friederichs, and M. Latif, 2004: Tropical Pacific decadal variability and its relation to decadal modulations of ENSO. *J. Climate,* **17,** 3761–3774.

Santoso, A., W. Cai, M. H. England, and S. J. Phipps, 2011: The role of the Indonesian Throughflow on ENSO dynamics in a coupled climate model. *J. Climate,* **24,** 585–601.

——, M. H. England, and W. Cai, 2012: Impact of Indo-Pacific feedback interactions on ENSO dynamics diagnosed using ensemble climate simulations. *J. Climate,* **25,** 7743–7763.

Vincent, E. M., and Coauthors, 2011: Interannual variability of the South Pacific convergence zone and implications for tropical cyclone genesis. *Climate Dyn.,* **36,** 1881–1896.

Vos, R., M. Velasco, and E. de Labastida, 1999: Economic and social effects of El Niño in Ecuador, 1997–1998. Inter-American Development Bank, Sustainable Development Dept. Tech. Paper POV-107, 38 pp.

Wang, B., R. Wu, and R. Lukas, 1999: Roles of the western North Pacific wind variations in thermocline adjustment and ENSO phase transition. *J. Meteor. Soc. Japan,* **77,** 1–16.

Weisberg, R. H., and C. Wang, 1997: A western Pacific oscillator paradigm for the El Niño–Southern Oscillation. *Geophys. Res. Lett.,* **24,** 779–782.

Wittenberg, A. T., 2009: Are historical records sufficient to constrain ENSO simulations? *Geophys. Res. Lett.,* **36,** L12702, doi:10.1029/2009GL038710.

Yeh, S.-W., J.-S. Kug, B. Dewitte, M.-H. Kwon, B. Kirtman, and F.-F. Jin, 2009: El Niño in a changing climate. *Nature,* **461,** 511–514, doi:10.1038/nature08316.